

Sliding ferroelectric tunneling junctions with large electroresistance ratio

Xinyu Lv(吕新裕), Ming Lv(吕铭), Jian Liao(廖健), Ming Tian(田明), Neng Wan(万能), Jiamin Xue(薛加民)
Citation: Chin. Phys. B. 35, 097701 (2026). DOI: 10.1088/1674-1056/ae6f99 |
CSTR: 32038.14.CPB.ae6f99
http://cpb.iphy.ac.cn; http://iopscience.iop.org/cpb

What follows is a list of articles you may be interested in

Generalized likelihood ratio detector for forward scattering detection in uncertain sha llow-water environments

Jiahui Luo(罗嘉辉), Chao Sun(孙超), Mingyang Li(李明杨), Shaodong Zhang(张少东)
Chin. Phys. B. 35, 054303 (2026). DOI: 10.1088/1674-1056/ae118f | CSTR: 32038.14.CPB.ae118f

Cascaded deep UV and blue LEDs with integrated GaN tunnel junction

Amina Hafeez, Muhammad Usman, Hazrat Ali, Jamshad Bashir, Zoya Noor
Chin. Phys. B. 35, 057302 (2026). DOI: 10.1088/1674-1056/ae32fd | CSTR: 32038.14.CPB.ae32fd

Enhanced photon emission by field emission resonances and local surface plasmon in tunneling junction

Jian-Mei Li(李健梅), Dong Hao(郝东), Li-Huan Sun(孙丽欢), Xiang-Qian Tang(唐向前), Yang An(安旸), Xin-Yan Shan(单欣岩), Xing-Hua Lu(陆兴华)
Chin. Phys. B. 31, 116801 (2022). DOI: 10.1088/1674-1056/ac8732

Recent advances, perspectives, and challenges inferroelectric synapses

Bo-Bo Tian(田博博), Ni Zhong(钟妮), Chun-Gang Duan(段纯刚)
Chin. Phys. B. 29, 097701 (2020). DOI: 10.1088/1674-1056/aba603

RAPID COMMUNICATION

Sliding ferroelectric tunneling junctions with large electroresistance ratio

Xinyu Lv(吕新裕)[1], Ming Lv(吕铭)[1], Jian Liao(廖健)[1],
Ming Tian(田明)[2,†], Neng Wan(万能)[2,4,‡], and Jiamin Xue(薛加民)[1,3,§]

[1] *School of Physical Science and Technology, ShanghaiTech University, Shanghai* 201210, *China*
[2] *Key Laboratory of MEMS of Ministry of Education, College of Integrated Circuits, Southeast University, Nanjing* 210096, *China*
[3] *State Key Laboratory of Quantum Functional Materials, ShanghaiTech University, Shanghai* 201210, *China*
[4] *State Key Laboratory of Surface Physics, Key Laboratory of Micro and Nano Photonic Structures (MOE), and Department of Physics, Fudan University, Shanghai* 200433, *China*

(Received 9 April 2026; revised manuscript received 7 May 2026; accepted manuscript online 19 May 2026)

Sliding ferroelectric materials such as twisted hexagonal boron nitride (tw-hBN) have the advantages of fast switching and fatigue resistance compared with conventional ferroelectrics. However, their polarization is orders of magnitude lower than that of conventional ferroelectrics. Therefore, tunneling junctions based on sliding ferroelectrics usually have a low electroresistance ratio of order 1, due to a marginal modulation of the tunneling barrier by the weak polarization. Here we show that the polarization in tw-hBN can cause a significant shift of the band edges in a few-layer $MoSe_2$ electrode by ~ 0.2 eV and result in an electroresistance ratio of ~ 100. We clarify that the density of states in $MoSe_2$ instead of the tunneling barrier dominates the electroresistance ratio enhancement. Our study provides a viable route of utilizing sliding ferroelectrics in fast switching and high endurance non-volatile memories. In addition, the large band modulation capability of tw-hBN demonstrated in this work provides an attractive tool for engineering band structures in layered semiconductors.

Keywords: liding ferroelectrics, ferroelectric tunneling junction, electroresistance ratio

PACS: 77.80.–e, 73.40.Gk, 77.80.Fm

DOI: 10.1088/1674-1056/ae6f99 **CSTR:** 32038.14.CPB.ae6f99

Sliding ferroelectric materials have been a recent research focus due to their intriguing properties.[1–5] First, the electrical polarization results from the electron wave function redistribution between atomic layers, which can be induced in various non-polar materials through stacking engineering.[6] Second, the polarization switching is realized by a superlubric domain wall movement, leading to an ultrafast and fatigue-free switching process.[3,7–9] The atomically thin thickness of these sliding ferroelectric materials makes them natural candidates for the tunneling layer in ferroelectric tunneling junctions (FTJs).

FTJs represent a type of non-volatile memory device. The polarization of a thin ferroelectric material sandwiched between two metallic electrodes modulates the resistance R through the device.[10] An important figure of merit is the tunneling electroresistance ratio (TER), defined as TER $= (R_{\rm high} - R_{\rm low})/R_{\rm low}$. Two mechanisms have been proposed to enhance the TER with great success for conventional displacive ferroelectrics, namely the height or width modulation of the tunneling barrier.[10,11] However, due to their low polarization (usually a couple of orders smaller compared with that of ionic displacive ferroelectrics[6]), FTJs based on sliding ferroelectrics have only shown a TER of order 1 or less,[12,13] far inferior to the FTJs based on displacive ferroelectrics.

In this study, we show that the conventional mechanism for modulating the tunneling barrier is ineffective for sliding ferroelectric FTJs based on twisted hexagonal boron nitride (tw-hBN). On the other hand, the polarization in tw-hBN induced band structure change of a $MoSe_2$ electrode could be exploited to realize a TER of 100. The major factor responsible for this large TER is found to be a band edge shift of ~ 0.2 eV in $MoSe_2$ modulated by the polarization switching. Combined with their inherent fast switching and high endurance, our work thus demonstrates the great potential of sliding ferroelectrics in FTJ applications. The band edge modulation induced by the moire domains in tw-hBN also provides an attractive platform for band structure engineering in layered semiconductors.

We chose tw-hBN as the sliding ferroelectric layer, which has the largest polarization of ~ 0.68 μC·cm^{-2} among the reported sliding ferroelectric materials.[6] The schematic diagram of the FTJ device investigated in this study is shown in Fig. 1(a). The 0.66-nm-thick tw-hBN is placed on a few-layer

†Corresponding author. E-mail: 651441756@qq.com
‡Corresponding author. E-mail: 101011244@seu.edu.cn
§Corresponding author. E-mail: xuejm@shanghaitech.edu.cn

© 2026 Chinese Physical Society and IOP Publishing Ltd. All rights, including for text and data mining, AI training, and similar technologies, are reserved.

$MoSe_2$ bottom electrode, and a conductive atomic force microscopy (CAFM) tip acts as the top electrode. The $MoSe_2$ and tw-hBN stack is placed on a thick graphite substrate (> 50 nm) to ensure optimal electrical contact and surface flatness. During electrical measurements, the bias voltage was applied to the $MoSe_2$ electrode through the graphite substrate with the AFM tip grounded.

Recent studies have demonstrated that Kelvin probe force microscopy (KPFM) serves as a critical methodology for verifying the ferroelectric domains of tw-hBN.[14,15] Figure 1(b) presents the KPFM characterization of a typical device, showing that the relaxed tw-hBN forms triangular domains with distinct surface potential variations, which are induced by alternating out-of-plane polarization in neighboring domains. This result is consistent with previous observations[14] and confirms that the sliding ferroelectric polarization has been developed in our devices.

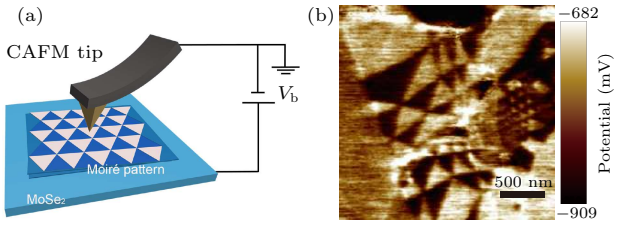


Fig. 1. FTJ schematic and confirmation of polarization domains. (a) Schematic diagram of the experimental setup. (b) KPFM potential image of a tw-hBN device showing triangular domains produced by alternating out-of-plane polarization.

To demonstrate that the weak polarization in tw-hBN is inefficient for tuning the tunneling barrier, we fabricated an FTJ with graphene as the bottom electrode. A graphene electrode has been adopted in a $CuInP_2S_6$ FTJ before[16] to realize a giant TER of 10^7. This effect is due to a large shift of the Fermi level in graphene (therefore the tunnel barrier height) of ~ 1 eV induced by the polarization switching in $CuInP_2S_6$. A CAFM scan of tw-hBN on graphene is shown in Fig. 2(a), presenting two types of domains with high and low current, respectively. This pattern is similar to that obtained with KPFM (Fig. 1(b)), demonstrating that polarization in tw-hBN is modulating the tunneling resistance. However, two *I*–*V* curves measured at the centers of the high- and low-current domains (represented by the blue and red points, respectively, in Fig. 2(a)) reveal the weak modulation with a TER of ~ 2. This result aligns with our previous findings in devices of tw-hBN on a thick graphite electrode[17] but shows significant divergence from the $CuInP_2S_6$/graphene FTJ. This discrepancy has two origins. First, the polarization strength in tw-hBN (0.68 $\mu C \cdot cm^{-2}$) is weaker than that of $CuInP_2S_6$ (8 $\mu C \cdot cm^{-2}$).[16] As a result, the change of the tunneling barrier height induced by the polarization switching is small. Second, the ferroelectric layer (tw-hBN) is atomically thin, further reducing the effect of barrier height change. To see these factors more clearly, we performed calculations based on the direct tunneling theory as shown in the supplementary material S1. The calculated TER of a tw-hBN/graphene FTJ is only ~ 1.3, consistent with our experimental observations and previous reports.[12,13]

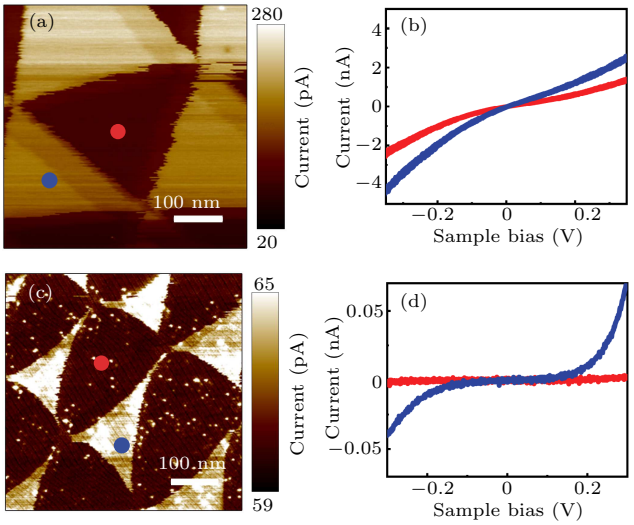


Fig. 2. Comparison of FTJ properties with different electrodes. (a) CAFM image of graphene-electrode device with 50 mV sample bias voltage. (b) Tunneling *I*–*V* curves at the two domains with opposite polarizations indicated by the red and blue dots in (a). (c) CAFM image of $MoSe_2$-electrode device with 600 mV sample bias voltage. (d) Tunneling *I*–*V* curves at two domains with opposite polarizations indicated by the red and blue dots in (c).

Having established that tw-hBN is inefficient at tuning the tunneling barrier in an FTJ with a graphene electrode, we replace the graphene with a few-layer semiconducting $MoSe_2$ electrode. A prior theoretical study demonstrated that the ferroelectric polarization in tw-hBN can induce significant modulation to the electronic band structure of adjacent $MoSe_2$ layers.[14] This modulation has the potential to strongly impact the behavior of an FTJ incorporating a tw-hBN/$MoSe_2$ structure. In FTJs based on conventional ionic ferroelectric materials, heavily doped semiconductors have been used as the electrode to achieve high TER,[11,18] resulting from the polarization-switching-induced depletion width change in the semiconductor electrode. Therefore, it is the tunneling barrier width modulation that contributes to the high TER. However, considering its weak polarization demonstrated in Fig. 2(b), tw-hBN has limited capability of tuning the depletion width in a semiconductor electrode. As we will show later, tw-hBN/$MoSe_2$ FTJs rely on the band edge shift of $MoSe_2$ to realize a high TER.

Figure 2(c) presents the CAFM mapping of tw-hBN on a trilayer $MoSe_2$. The domains are clearly visible with bright dots, which could be defects in $MoSe_2$. The tunneling *I*–*V* curves at the high- and low-current domains (represented by the blue and red points, respectively, in Fig. 2(c)) are shown in Fig. 2(d). It is evident that the two curves behave rather

differently. The red curve exhibits a markedly reduced current across the entire applied voltage range, corresponding to a pronounced enhancement in the TER relative to the tw-hBN/graphene device (Fig. 2(b)).

To investigate the mechanism underlying the observed TER enhancement, $\mathrm{d}I/\mathrm{d}V$ spectroscopy measurements, as shown in Fig. 3(a), were taken along a line crossing two domains. These spectra were acquired at 3-nm intervals as the tip moved across a domain wall. The black dotted box highlights the spectra of the domain wall region with clear hysteresis, which will be discussed in Fig. 4. The left part of Fig. 3(a) corresponds to the low-current domain, characterized by an extensive voltage range (the blue area) with close-to-zero $\mathrm{d}I/\mathrm{d}V$ value. Since in a tunneling process $\mathrm{d}I/\mathrm{d}V$ is proportional to the DOS in the sample, this zero-$\mathrm{d}I/\mathrm{d}V$ region can be attributed to the intrinsic band gap of $MoSe_2$. When the tip moved across the domain wall into the high-current domain, a sudden reduction of the band gap region signifies the consequence of the polarization switching in tw-hBN.

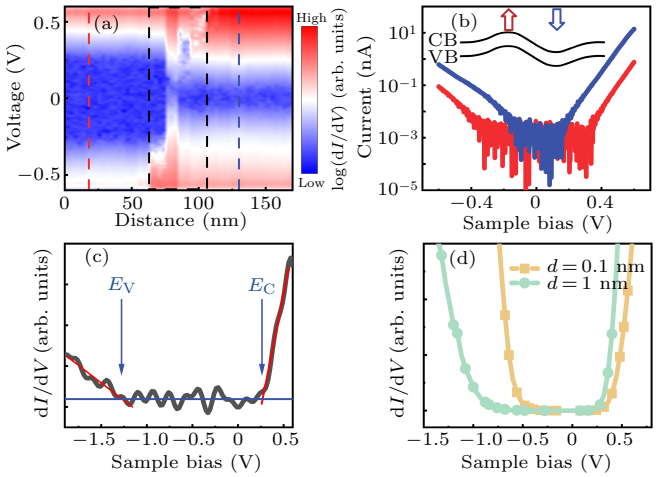


Fig. 3. Analysis of the *I*–*V* curves of the device shown in Fig. 2(a). (a) $\mathrm{d}I/\mathrm{d}V$ spectra across a domain wall. The black dotted box circles out the domain wall region where hysteresis can be observed, which will be discussed in Fig. 4. (b) Log-scale *I*–*V* curves at two domains with opposite polarizations, as marked by the red and blue dotted lines in (a). Inset: Schematic for polarization induced band edge shift. (c) A conventional STS spectrum of $MoSe_2$. STS current setpoint: 15 pA. (d) Simulation results of $\mathrm{d}I/\mathrm{d}V$ curves with different tip-sample distances.

Figure 3(b) displays logarithmic-scale *I*–*V* curves acquired at the high- and low-current domains with positions shown by the blue and red dotted lines in Fig. 3(a), respectively. For the blue *I*–*V* curve, current increases exponentially with voltage exceeding ±150 mV, whereas the red *I*–*V* curve exhibits a significantly elevated activation threshold of ±350 mV. A significant TER of ∼ 100 can be seen in the positive voltage range, which is much higher than that of other FTJs based on sliding ferroelectrics (see supplementary material S2 for a detailed comparison).[17] The mechanism of the ferroelectric-polarization-modulated tunneling process is revealed by the line shapes of these two curves, which exhibit two salient features. First, the *I*–*V* curves have a gap feature around zero sample bias voltage. Second, outside this gap region, the two *I*–*V* curves are nearly parallel. In FTJs based on conventional ferroelectric materials and semiconductor electrodes,[11,18] the *I*–*V* curves of the high- and low-current states usually show very different line shapes (in logarithmic-scale plots similar to that of Fig. 3(b)), since in those FTJs the tunneling barrier width and/or height are significantly modulated by the polarization switching. Here, the nearly parallel *I*–*V* curves, especially in the positive bias range, indicate that the tunneling barrier is almost the same for the two polarization states. Due to the presence of the gap, we attribute the exponential increase in current in the positive bias range to tunneling into the conduction band of $MoSe_2$. From Fig. 3(b), the conduction band edge can be extracted to be 150 meV for the high-current state and 350 meV for the low-current state. This assignment is further corroborated by theoretical calculations and conventional scanning tunneling spectroscopy (STS) measurements. Previous theoretical studies have evaluated the effect of ferroelectric polarization of tw-hBN on the band edges of $MoSe_2$ in contact with the tw-hBN,[14] and showed that the conduction and valence band edges can be shifted down or up by ∼ 100 meV when the polarization in tw-hBN points towards or away from the MoS_2, respectively (as schematically shown in the inset of Fig. 3(b)). In addition, conventional ultrahigh vacuum STS on the exfoliated surface of $MoSe_2$ (Fig. 3(c)) showed that the conduction band edge of bare $MoSe_2$ is located at 250 meV, halfway between the values measured in Fig. 3(b), and in quantitative agreement with the theoretical expectation. These results confirm that the high TER observed in this device structure originates from the band edge shift as schematically shown in the inset of Fig. 3(b), rather than tunneling barrier modification. Schematic band diagrams and more detailed discussions for the high-current and low-current states are provided in the supplementary material S3.

A notable feature in Fig. 3(b) warrants further discussion. Conventional STS in Fig. 3(c) measures a band gap of ∼ 1.5 eV in $MoSe_2$, with the valence band edge located at ∼ −1.25 eV. In contrast, the gap size shown in Fig. 3(b) is much smaller, with the valence band edge located significantly closer to the Fermi level (zero sample bias). We attribute this discrepancy to a tip-induced band bending effect[19] arising from the narrow tip-$MoSe_2$ distance. Figure 3(d) presents a self-consistent Schrödinger-Poisson simulation[20] of the $\mathrm{d}I/\mathrm{d}V$ spectra of an n-type semiconductor at two different tip-sample distances. When the distance is reduced from the normal tunneling range of 1 nm to 0.1 nm, the conduction band edge remains at almost the same position while the valence band edge shifts upward in energy significantly (see the supplementary material S4 for calculation details). In our FTJ structure, the tunneling barrier consists of the 0.66-nm-thick

tw-hBN. Considering the dielectric constant of about 3.58 for hBN,[21] the effective distance between the CAFM tip and $MoSe_2$ is about 0.18 nm, which is similar to that used for simulation. Therefore, the discrepancy between Figs. 3(b) and 3(c) can be reconciled.

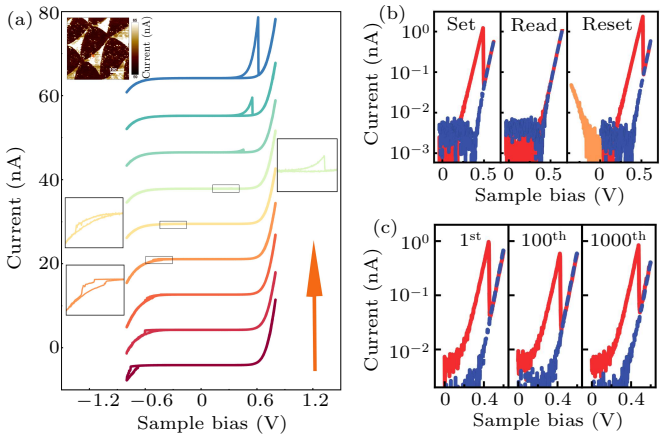


Fig. 4. Hysteresis behavior of the FTJ. (a) *I*–*V* curves across a domain wall with 3 nm interval between successive curves. They are displayed with a vertical shift for clarity. The arrow in the main panel indicates the spatial sequence of the measurements, corresponding to the arrow in the inset. The starting position of the first *I*–*V* curve is approximately 23 nm away from the domain wall. (b) Log-scale *I*–*V* curves showing non-volatile memory behavior. (c) Endurance test over 1000 voltage sweeping cycles.

Having established the band edge shift as the mechanism for the significantly enhanced TER, we explore the switching of the polarization and the associated tunneling current modulation. As shown in Fig. 4(a), *I*–*V* curves around the domain wall region, highlighted by the black dotted box in Fig. 3(a), reveal sudden jumps and hysteresis in the current. Our previous work on tw-hBN on graphite electrodes[17] has demonstrated similar behaviors, which were identified as electric-field-induced polarization switching. The spatial dependence of the current jump positions (i.e., the coercive field) signifies the polarization switching dynamics determined by local lattice symmetry.[4,17,22] As the tip moves away from the domain wall, the current peak becomes higher, resulting from the larger coercive field.

Near the domain wall, the polarization switching hysteresis is non-volatile, as more clearly illustrated in Fig. 4(b) (see supplementary material for CAFM mappings). In the first and second panels of Fig. 4(b), the bias voltage sweep is restricted to positive polarities. A current jump at ~ 0.5 V is shown in the first panel when the bias voltage is swept from 0 to 0.6 V (red part of the curve), after which the tunneling junction is set to a low-current state (blue part of the curve). A subsequent reading sweep confirms the retention of the low-current state (second panel). In the reset process (third panel), the bias voltage is first swept to -0.3 V (yellow part of the curve). Upon sweeping back to positive biases, the tunneling junction returns to the high-current state (red part of the curve), which subsequently switches back to the low-current state (blue part of the curve), as evidenced by the current jump and hysteresis loop. We note that the reset occurred in the gap region, so no current jump can be detected. In some measurements, the reset current jump can be clearly seen (see Fig. S5 in supplementary material for an example).

One of the characteristic properties of sliding ferroelectrics is the high endurance, arising from their fatigue-free polarization switching behavior. While in our current FTJ structure, the CAFM tip drift prevents maintaining the tip at the exact same position for prolonged measurements, we nevertheless attempted to evaluate the device endurance. As shown in Fig. 4(c), the *I*–*V* curves from 1000 cycles of bias-voltage sweeping are shown with excellent consistency. The slope variations of the high- and low-current *I*–*V* curves are within 2.5% and 1.6% of their initial values, respectively, indicating the long-term stability of the tunneling junction based on tw-hBN. In fact, studies have already demonstrated that the ferroelectric performance of twisted hBN-based field-effect transistors can be maintained for up to 10^{11} cycles,[3] which is due to the intrinsic properties of hBN and realized through superlubric domain wall propagation.[4]

In conclusion, we have demonstrated the FTJs based on the sliding ferroelectric material tw-hBN with $MoSe_2$ as one of the electrodes. By leveraging the ferroelectric-polarization-modulated band edges, a TER of ~ 100 can be achieved, despite the weak polarization in sliding ferroelectrics. Beyond the potential implications for future FTJ studies, this work also precisely determined the conduction band edge shift of $MoSe_2$ induced by tw-hBN to be ~ 200 meV. This large modulation demonstrates the potential of tw-hBN in controlling the electronic properties in layered semiconductors, as recently evidenced by the optical measurements of $MoSe_2$ modulated by the ferroelectric domains in tw-hBN.[14,23]

Supplementary material

Numerical simulation results of the *I*–*V* curves based on the direct tunneling model; comparison of the on/off ratios of different sliding ferroelectric devices; schematic band diagrams of the devices and related discussions; parameter settings for the TIBB numerical calculations; demonstration of the device non-volatility in CAFM mapping are presented in supplementary material.

Acknowledgements

The authors thank the Soft Nano Fabrication Center and Dr. Xinyan Wang at ShanghaiTech University for the equipment provided. J.X. was supported by the National Natural Science Foundation of China (Grant No. 12374189). N.W. thank the supporting from the Open Project of Key Laboratory of Artificial Structures and Quantum Control (Ministry of Ed-

ucation), Shanghai Jiao Tong University, M.T. thank the Postgraduate Research & Practice Innovation program of Jiangsu Province (Grant No. KYCX22_0228).

References

[1] Vizner S M, Waschitz Y, Cao W, Nevo I, Watanabe K, Taniguchi T, Sela E, Urbakh M, Hod O and Ben Shalom M 2021 *Science* **372** 1462

[2] Yasuda K, Wang X, Watanabe K, Taniguchi T and Jarillo-Herrero P 2021 *Science* **372** 1458

[3] Yasuda K, Zalys-Geller E, Wang X, Bennett D, Cheema S S, Watanabe K, Taniguchi T, Kaxiras E, Jarillo-Herrero P and Ashoori R 2024 *Science* **385** 53

[4] Ke C, Liu F and Liu S 2025 *Phys. Rev. Lett.* **135** 046201

[5] Liu Y, Liu G 2024 *Chin. Phys. B* **34** 17701

[6] Li L and Wu M 2017 *ACS Nano* **11** 6382

[7] Yang Q, Meng S 2024 *Phys. Rev. Lett.* **133** 136902

[8] Wang J, Li X, Ma X, Chen L, Liu J M, Duan C G, Íñiguez-González J, Wu D, Yang Y 2024 *Phys. Rev. Lett.* **133** 126801

[9] Bian R, He R, Pan E, Li Z, Cao G, Meng P, Chen J, Liu Q, Zhong Z, Li W and Liu F 2024 *Science* **385** 57

[10] Zhuravlev M Ye, Sabirianov R F, Jaswal S S and Tsymbal E Y 2005 *Phys. Rev. Lett.* **94** 246802

[11] Wen Z, Li C, Wu D, Li A and Ming N 2013 *Nat. Mater.* **12** 617

[12] Wan Y, Hu T, Mao X, Fu J, Yuan K, Song Y, Gan X, Xu X, Xue M, Cheng X, Huang C, Yang J, Dai L, Zeng H and Kan E 2022 *Phys. Rev. Lett.* **128** 067601

[13] Gao Y, Weston A, Enaldiev V, Li X, Wang W, Nunn J E, Soltero I, Castanon E G, Carl A, De Latour H, Summerfield A, Hamer M, Howarth J, Clark N, Wilson N R, Kretinin A V, Fal'ko V I and Gorbachev R 2024 *Nat. Commun.* **15** 4449

[14] Kim D S, Dominguez R C, Mayorga-Luna R, Ye D, Embley J, Tan T, Ni Y, Liu Z, Ford M, Gao F Y, Arash S, Watanabe K, Taniguchi T, Kim S, Shih C K, Lai K, Yao W, Yang L, Li X and Miyahara Y 2024 *Nat. Mater.* **23** 65

[15] Cho M, Datta B, Han K, Chand S B, Adak P C, Yu S, Li F, Watanabe K, Taniguchi T, Hone J, Jung J, Grosso G, Kim Y D and Menon V M 2025 *Nano Lett.* **25** 1381

[16] Wu J, Chen H Y, Yang N, Cao J, Yan X, Liu F, Sun Q, Ling X, Guo J and Wang H 2020 *Nat. Electron.* **3** 466

[17] Lv M, Sun X, Chen Y, Taniguchi T, Watanabe K, Wu M, Wang J and Xue J 2022 *Adv. Mater.* **34** 2203990

[18] Jin Hu W, Wang Z, Yu W and Wu T 2016 *Nat. Commun.* **7** 10808

[19] Feenstra R M, Dong Y, Semtsiv M P and Masselink W T 2006 *Nanotechnology* **18** 044015

[20] Ishida N, Sueoka K and Feenstra R M 2009 *Phys. Rev. B* **80** 075320

[21] Laturia A, Van de Put M L and Vandenberghe W G 2018 *npj 2D Mater. Appl.* **2** 6

[22] Wang Z and Dong S 2025 *Phys. Rev. B* **111** L201406

[23] Kim D S, Xiao C, Dominguez R C, Liu Z, Abudayyeh H, Lee K, Mayorga-Luna R, Kim H, Watanabe K, Taniguchi T, Shih C K, Miyahara Y, Yao W and Li X 2025 *Sci. Adv.* **11** eadt7789